Plasma Plume Effect in Laser Welding under Subatmospheric Pressure

Jingyue Zhang[1,a,*]

[1]*School of Physical Science and Technology, Southwest University, Chongqing, 400715, China*
a. 956342063@qq.com
*corresponding author

Abstract: In laser welding, the plasma plume often shields the input energy, causing laser beam defocusing and significantly impacting welding efficiency and quality. This paper elucidates experimental facts concerning the attenuation and dispersion of laser energy at varying ambient pressures, and derives the associated absorption and refraction mechanisms of the plasma plume. By analyzing experimental and simulation results from scholars, the mechanism by which laser-plasma interaction affects weld formation is illustrated. A comprehensive analysis is conducted on the impact of ambient pressure and welding speed on weld morphology. The conclusion drawn is that there is a good correspondence between the influence of ambient pressure on melting depth and plasma plume, with a material-dependent critical pressure value. Furthermore, higher welding speeds decouple ambient pressure from weld depth but contribute to reducing porosity defects. Therefore, appropriate welding speeds and ambient pressures should be selected based on actual industrial application scenarios. Finally, the paper suggests future research on LWSP should focus on real-time monitoring with multi-sensor fusion, optimizing machine learning models, exploring novel imaging techniques, and combining LWSP with hybrid welding.

Keywords: Vacuum Laser Welding, Subatmospheric Pressure, Plasma Plume, Cross-section Morphology, Welding Speed

1. Introduction

Laser welding, noted for its high energy density, precision, and minimal deformation, is prevalent in electronics and nuclear power applications. However, the laser-induced plasma plume obstructs the beam and degrades welding quality. Current suppression methods include laser scanning with wobble (LSSW), electromagnetic field control, side gas blowing, shielding gas modification, and subatmospheric laser welding (LSWP) [1-4]. Among these, LWSP has emerged as a promising method, yet it has garnered insufficient attention from both academia and industry [5]. Plasma plume behavior fluctuates with ambient pressure, affecting welding processes. Despite extensive research on control, understanding of its sub-atmospheric dynamics and weld formation effects remains limited. Further exploration of ambient pressure's impact on plasma characteristics and laser welding quality is needed. This paper analyzes experimental phenomena and theoretical derivations to elucidate laser-plasma interactions across diverse ambient pressures. It comprehensively summarizes and analyzes experimental and simulation findings, exploring mechanisms influencing laser welding and formation. The impact of ambient pressure and welding speed on weld morphology is examined.

The research concludes with recommendations for enhancing laser sub-atmospheric LSWP technology. The research enhances laser welding efficiency and quality, benefiting manufacturing, engineering, and industries reliant on high-precision welding, by elucidating plasma plume effects and optimizing welding parameters.

2. Laser Induced Plume

Upon laser impact on a metal sheet, electrons absorb energy, causing temperature rise, melting, and evaporation. High evaporation results in recoil pressure, forming a deep cavity (keyhole). This ejects neutral metal atoms, forming ultrafine particles or fumes that glow brightly at high temperatures, termed laser-induced plumes. At high laser energy, these substances become laser-induced plasma [6]. Evaporated atoms form clusters and ultrafine particles, visible as fumes above the workpiece.

Laser-Plasma interaction mainly includes the following four aspects.

Absorption

Laser light through plasma loses energy via normal (inverse bremsstrahlung) and anomalous absorption. Lambert-Beer law quantifies laser intensity reduction post-plasma traversal.

$$I = I_0 \left(- \int_0^L \frac{\pi}{4} C_n \left(\int_0^\infty Q_{abs} N(a) a^2 da \right) dl \right) \tag{1}$$

In Equation (1), I_0 is the initial intensity of the incident laser; L is the height through which the laser passes through the plasma. C_n represents the number density of the plasma plume, Q_{abs} denotes the absorption efficiency for a single plasma plume particle, and N(a) is the particle size distribution function satisfying the condition $\int N(a) da = 1$.

Scattering

The plasma plume generated by the interaction between laser light and metal contains a large number of ultrafine particles formed by the condensation of metal vapor atoms. The particles scatter the incident laser beam, and the scattering loss is inversely related to the fourth power of the wavelength of the incident light. Shorter laser wavelengths enhance scattering for particles of equal size.

Reflection

Reflection occurs at the plasma surface or interfaces. The degree of reflection depends on interface properties and the laser's incidence angle. Plasma generation alters the reflectivity of the target surface due to its distinct optical properties compared to the target material, leading to an increase or decrease in reflectivity. It effect weakens the energy of laser welding.

Refraction

Uneven electron density causes refractive index variation, leading to laser divergence, spot size expansion, and reduced energy density. The plasma plume acts as a negative lens. For an estimation of this effect, the deflection angle θ of the laser beam is quantified using previous studies on electron density and can be expressed as:

$$\theta = \frac{\nabla N_e}{2N_{ec}} L = \frac{N_e}{2N_{ec}} \frac{L}{R} \tag{2}$$

In Equation (2), R represents the radius of the plasma plume, ∇N_e is the gradient of the electron density, and N_{ec} is the critical cutoff density depending on the laser wavelength. N_e represents the electron density at the center of the plasma plume.

3. Ambient Pressure on the Interaction between Laser and Plasma Plume

A study indicates that during deep penetration welding, the laser-induced plasma plume primarily interacts with the laser through absorption and refraction effects [7]. Therefore, this chapter explores plasma plume absorption and refraction under various pressures, assessing their laser interactions and their impact on laser welding formation.

3.1. Absorption and Refraction Effects under Different Environmental Pressures

Kurita et al. conducted laser welding experiments under varying pressures in 2023, using a 1064 nm probe laser perpendicular to the welding laser [8]. The probe laser traversed a vacuum chamber, passing through a filter and received by a photodiode, with signals sampled at 1.0×10^6 Hz. A positive correlation between ambient pressure and probe laser attenuation, with rates ranging from 7.2% at 0.1 kPa to 51.3% at 100 kPa. Higher pressures enhanced absorption and scattering of the laser-induced plume, impacting laser energy input, energy transfer, and welding outcomes.

In 2021, Gong et al. utilized probe laser technology to study laser energy dispersion, finding that plasma plume-induced refraction affected laser spot size and position [9]. The mean size and deflection angle of the laser spot were sensitive to ambient pressure, decreasing with lower pressure. At 100 kPa, the average area and deflection angle were 5.48 mm² and 1.22 mrad, respectively, compared to 3.12 mm² and 0.118 mrad at 0.01 kPa(Figure 1).
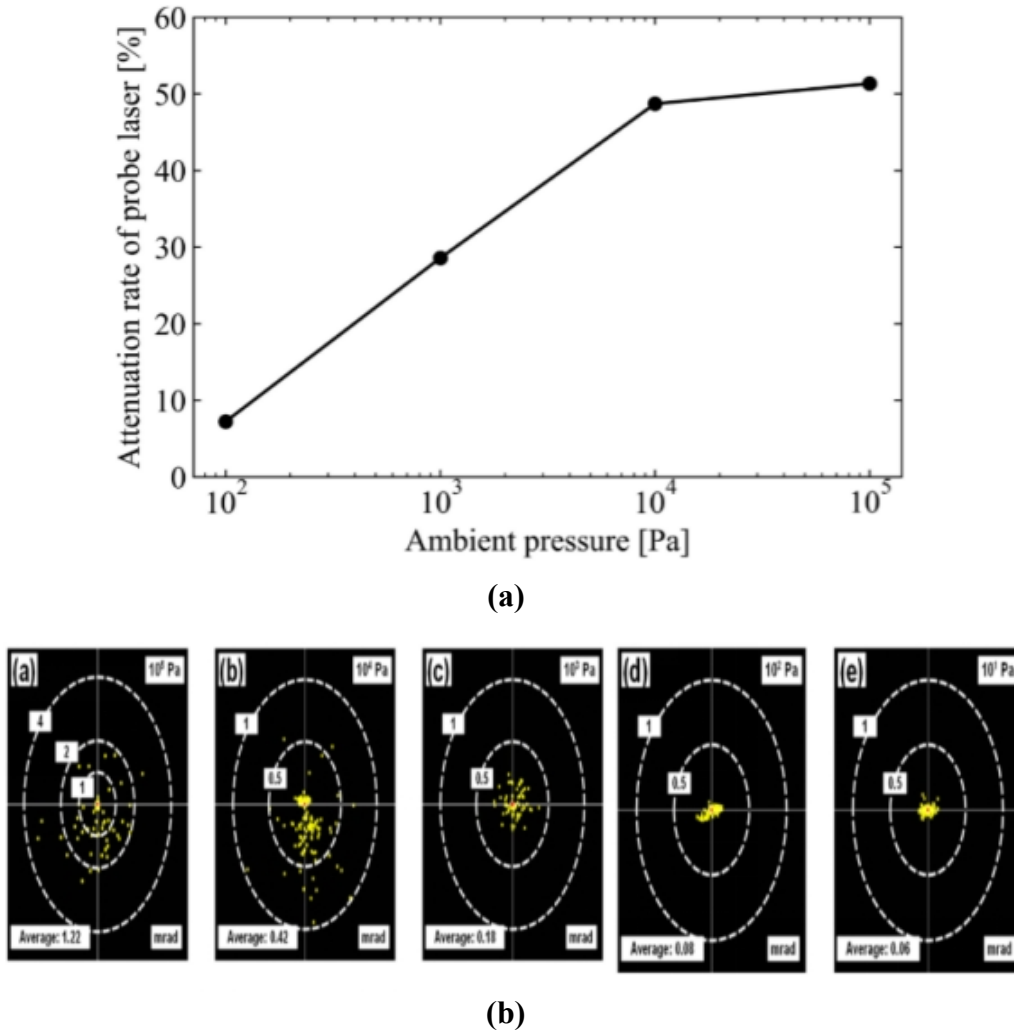

(a)

(b)

Figure 1: Laser energy attenuation and distribution under different ambient pressures (a) Attenuation rate of probe laser with different ambient pressures of 0.1, 1,10, and 100 kPa. [8] (b) Positons distribution and refractive angles under different ambient pressures [9]

Based on Kurita's experiments, it is evident that as ambient pressure increases, the plasma plume leads to an elevated attenuation rate of the 1064 nm probe laser, subsequently affecting laser energy

transfer. Gong et al.'s 2021 study further revealed that the plasma plume alters the size and position of the laser spot through refraction effects, with both the average area and deflection angle of the laser spot decreasing as pressure decreases, indicating a weakened refraction of laser light by the plasma plume in low-pressure environments, thereby enhancing the stability of laser energy density. Consequently, it can be deduced that in vacuum laser welding, the laser-plasma interaction predominantly affects the laser energy density and its distribution over the workpiece surface.

3.1.1. Analysis of Absorption Effect

The LTE equation for ionized plasma can be derived from the Saha equation:

$$\frac{n_e n_i}{n_0} = \frac{g_e g_i}{g_0} \frac{(2\pi m_e k T_e)^{3/2}}{h^3} \exp\left(\frac{-E_i}{kT_e}\right) \tag{3}$$

Where n_e, n_i, and n_0 represent the densities of electrons, ions, and neutral atoms, respectively; Te is the electron temperature; and g_e, g_i g_o, m_e, k, h, and E are constants. Assuming ideal gas plasma with uniform temp, the state equation is:

$$P = (n_0 + n_i + n_e)kT_e P = (n_0 + n_i + n_e)kT_e \tag{4}$$

The plasma vapor plume is overall electrically neutral and slightly ionized:

$$n_i = n_e << n_0 \tag{5}$$

Ultimately, the relationship between electron density and pressure P is derived as: [10]

$$n_e^2 = \frac{g_e g_i}{g_0 n_0^{1/2}} \frac{(2\pi m_e P)^{3/2}}{h^3} \exp\left(\frac{-E_i n_0}{P}\right) \tag{6}$$

Since the density of the plasma plume is directly proportional to the electron density, From (6), decreasing P leads to reduced electron and plasma densities. Inverse bremsstrahlung is the main laser absorption by plasma, with linear absorption coef. α expressed as:

$$\alpha = \frac{Z^2 e^6 n_e n_i \ln A}{12\pi^{7/2} c^3 \varepsilon_0 (2m_e k T_e)^{3/2}} \lambda^2 \tag{7}$$

Where Z is the ion charge number, lnA is the Coulomb logarithm, k is Boltzmann's constant, and Te is the electron temperature. Laser intensity I decays exponentially due to plasma absorption. For initial intensity I_0 through a plume of height L, I is derived by:

$$I = I_0 e^{-\alpha L} \tag{8}$$

Probe laser energy attenuation by plasma is described by Eq. (9)'s relative attenuation rate.

$$E = \frac{I_0 - I}{I_0} \tag{9}$$

Equation (8) shows that laser absorption by the plasma plume correlates with its electron density and altitude at a consistent electron temperature. Consequently, in the experiment shown in Figure 1(a), a reduction in ambient pressure results in diminished electron density and plasma plume height, thereby causing an increase in laser intensity I. Equation (9) indicates reduced relative extinction, suggesting a negative pressure environment decreases laser absorption by the plasma plume.

3.1.2. Analysis of Refraction Effect

Equation (2) shows that higher electron density and elongated plume enlarge the laser spot, broaden the interaction area, and decrease average intensity. Deviation is calculated by:

$$d = L\tan\left(\frac{N_e}{2N_{ec}} \frac{L}{R}\right) \tag{10}$$

Equation (10) suggests a dual influence of L on the deflection value. Under reduced pressure, L becomes more significant in determining energy distribution compared to the horizontal dimension R.

In the experiment depicted in Figure 1 (b), a decrease in ambient pressure leads to a reduction in electron density and its gradient inside the plume, resulting in a smaller plume size, which in turn

causes both d and θ to fall. This results in a diminished effect of the plasma plume on the positional distribution of the laser point and the deflection angle of its center position. Refraction modifies the size and location of the laser spot, whereas absorption primarily leads to a reduction in laser energy.
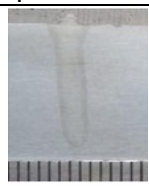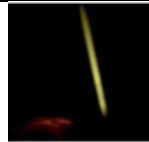
3.2. The Impact of the Interaction on the Laser Welding Formation

Laser-plasma interaction alters incident laser energy size and surface energy distribution, significantly impacting weld formation.

3.2.1. Experimental Result

Chen et al. performed a series of flat plate surface welding experiments at different ambient pressures (3, 10, 20, 35, and 101 kPa) with a travel speed of 1 m/min and a laser power of 8 kW [7]. An absolute pressure gauge was employed to measure the pressure in the vacuum chamber during welding, while a high-speed camera, positioned on the right side of the welding direction and operating at a frame rate of 1000 fps, recorded photos of the plasma plume. For welding processes within the range of 10-35 kPa, the same 8ND filter was employed for observation to obtain comparative information on plasma plume behavior. Table 1 shows a correlation between ambient pressure, plasma plume, and melting depth within a certain pressure range. Lower pressure reduces plasma volume, increases welding depth, and results in a "needle"-shaped cross-section.

Table 1: Cross-section profiles and plasma image of laser weldingwith the speed of 1 m/min and the power of 8 kW under various pressures [7]

Pressure (kPa)	3	10	20	35	101
ND filter	4	8	8	8	32
Cross section					
Weld zone (mm2)	53.1	45.1	39.3	38.6	38.3
Plasma image					
Scanning direction	→	→	→	→	→

In laser deep penetration welding, atmospheric pressure significantly affects metal vapor behavior and weld characteristics. At 101 kPa, heavy vapor accumulation around the keyhole blocks the laser beam, limiting penetration depth and resulting in a wide "nail-head"-shaped weld cross-section (53.1 mm²). Lowering pressure reduces vapor accumulation, enabling deeper laser penetration and producing a narrower "needle"-shaped weld cross-section (45.1-38.6 mm²). The reduced and stable vapor density facilitates controlled welding, enhancing weld quality and precision.
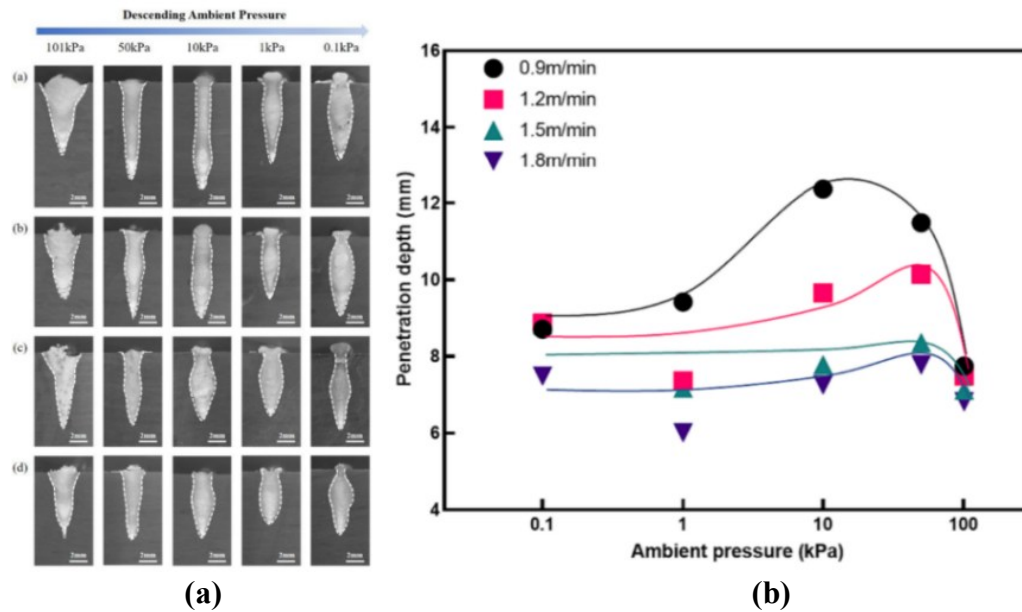
(a) **(b)**

Figure 2: Laser welding morphology of AZ31 Mg alloy at varied pressures and speeds. [11](A) Ambient pressure's impact on laser weld cross-section morphology at various speeds.(B)Ambient pressure's effect on weld penetration depth at various speeds and pressures.

Jiang et al. investigated the laser welding of AZ31 magnesium alloy under varying ambient pressures [12]. Figure 2(a) illustrates that, during overlay welding on a plate with a laser power of 3 kW and a focus of 0 mm, decreasing ambient pressure from 101 kPa to 10 kPa at different welding speeds resulted in a narrower and more uniform weld bead. Below 1 kPa, weld defects appeared, with hump defects occurring at 1 kPa and 0.1 kPa, worsening with increased welding speed. At atmospheric pressure, weld cross-sections were trapezoidal at various speeds. In vacuum, cross-sections were parallel-sided with high depth-to-width ratios at speeds below 1.2 m/min.

Figure 2(b) shows a sudden change in weld depth at various speeds. Penetration depth first increased then decreased as pressure dropped from 101 kPa to 0.1 kPa at speeds below 1.2 m/min; it did not enhance in vacuum at higher speeds. At 0.9m/min, penetration was 7.7 mm in air and 12.4 mm (1.6x) in a 10 kPa vacuum. At 1.2 m/min, it was 7.4 mm in air; at 1.8 m/min vacuum penetration resembled the 6.9 mm in air. Moreover, Jiang et al. also found that compared to Q345 steel and 5083 aluminum alloy, magnesium alasloy exhibited different trends in laser welding with varying environmental pressure, achieving maximum penetration and best weld formation at 10 kPa [11].

Consequently, it may be inferred that a critical value exists for the impact of ambient pressure on penetration depth, which correlates with the material's sensitivity to ambient pressure. Moreover, increased welding speeds make the ambient pressure independent of the welding depth.

3.2.2. Simulation Analysis

This section explores the causes of weld morphology changes in vacuum and the underlying mechanisms of welding speed's influence on weld appearance through existing simulation analysis.

Li et al. created a 3D model to study keyhole dynamics and melt flow in laser welding of 5A06 aluminum alloy [13]. At atmospheric pressure, keyhole wall temps varied from 1800-2700 K, impacting metal flow and weld morphology. Lower pressure reduced wall temps, narrowing temp differences with melting point, leading to a broader keyhole, stable pool, and better weld appearance. Fabbro et al. simulated weld penetration in vacuum, observing a decreasing penetration increase with welding speed [14]. Higher welding speeds elevate keyhole wall temperatures; at sufficiently high

speeds, these temperatures surpass boiling point and ambient pressure, rendering ambient pressure changes ineffective in altering metal evaporation temperature during high-speed welding. Li et al also illustrate that, at similar penetration depths, higher welding speeds weaken the vortices [13]. This weakening of vortices contributes to reducing porosity defects and enhancing welding stability. From the analysis, we conclude that within a pressure range, higher welding speeds reduce vortex behavior and porosity, stabilizing welds but excessively high speeds decrease penetration in vacuum.

4.   Suggestion for LWSP Development

Industry 4.0 has emphasized online monitoring and quality inspection of LW in sustainable smart manufacturing [15]. This section discusses the future research directions of LWSP.

Real-time Monitoring Using Multi-sensor Fusion Technology: Ma D et al. employed coherent optical diagnostics and a Deep Belief Network (DBN) in 2023 to identify pore areas during aluminum alloy laser welding, showcasing the technology's potential for real-time defect identification [12]. Multi-sensor fusion technology can further enhance the comprehensiveness and accuracy of real-time monitoring.

Optimization and Innovation of Machine Learning Models: Machine learning in welding is prevalent but confronts issues of accuracy, interpretability, and generalization. Cai W et al. proposed two deep learning methods in 2022: a U-Net algorithm for welding image segmentation and a lightweight CNN for penetration prediction [16]. Deep learning aids welding monitoring, suggesting future research for clarity and integration.

Exploration and Development of Novel Monitoring Methods: Traditional methods are limited in observing keyholes and molten pools, necessitating novel techniques like X-ray imaging, OCT, and metal-glass sandwich imaging. Sokolov M et al. demonstrated the high-precision potential of OCT in laser welding monitoring by applying it to automotive battery cell connector welding in 2021 [17].

Hybrid Welding Technology in Sub-Atmospheric Environments: LWSP has proven advantages and is anticipated to be integrated with other welding methods or energy sources, potentially enhancing welding outcomes such as joint strength, porosity reduction, and efficiency. LWSP with other welding techniques may solve welding challenges [5].

5.   Conclusion

This paper summarizes experimental phenomena concerning laser energy attenuation and distribution under various pressures, deriving plasma plume absorption and refraction mechanisms. It clarifies how laser-plasma interaction impacts weld formation through experimental and simulation analysis.

1. In vacuum laser welding, the plasma plume mainly influences the transmission of laser energy through refraction and absorption. Refraction alters the area and position of the laser spot, while absorption primarily causes the attenuation of laser energy.

2. In vacuum, laser welding plasma suppression enhances penetration and alters weld shape. Within a pressure range, ambient pressure correlates with melting depth and plasma behavior. A critical pressure affects penetration, related to material sensitivity. High welding speeds diminish pressure's influence on depth. Within a range, high speeds reduce porosity and enhance stability by weakening vortices. Thus, welding speeds and pressure should be tailored for industrial applications.

3. The future of laser welding lies in advancements in real-time monitoring, optimized machine learning, innovative techniques, and hybrid welding in sub-atmospheric environments, aiming to overcome limitations and provide tailored solutions for the manufacturing industry.

4. Besides weld morphology, laser-plasma interaction also affects the microstructure and mechanical properties of LWSP, which will be discussed in future research.

In conclusion, LWSP leverages unique benefits, with plasma plume, ambient pressure, and welding speed key to process quality and efficiency. Optimizing these ensures high-quality, consistent welds. Future research will expand applications, enhancing LWSP 's role in modern manufacturing.

References

[1] Arata, Y. (1987). Challenge of laser advanced materials processing. Proc. of LAMP, 87, 3-12.

[2] Tse, H. C., Man, H. C., & Yue, T. M.. (1999). Effect of electric and magnetic fields on plasma control during co2 laser welding. Optics and Lasers in Engineering, 32(1), 55-63.

[3] Wang C. M., Meng X. X., et al., 2011. "Role of side assisting gas on plasma and energy transmission during CO2 laser welding," Journal of Materials Processing Technology, Vol. 211, No. 4, pp. 668-674.

[4] Jiang, M., Tao, W., & Chen, Y.. (2017). Laser welding under vacuum: a review. Applied Sciences, 7(9), 909.

[5] Yang, F., Xia, G., Guo, X., Chen, C., & Chen, G.. (2021). Research progress of laser welding under subatmospheric pressure. The International Journal of Advanced Manufacturing Technology, 116(4), 1-18.

[6] Shevchik, S., Le-Quang, T., et al., 2020. "Supervised deep learning for real-time quality monitoring of laser welding with X-ray radiographic guidance," Sci Rep, Vol. 10, No. 1, pp. 1-12.

[7] Chen, Q., et al., 2015. "Study on the effect of laser-induced plasma plume on penetration in fiber laser welding under subatmospheric pressure," International Journal of Advanced Manufacturing Technology, Vol. 78, No. 1-4, pp. 331-339.

[8] Kurita, Y., Sato, Y., Fujio, S., Mizutani, M., & Tsukamoto, M. (2023). Influence of the laser-induced plume on welding behavior in keyhole welding for stainless steel using a 16 kW disk laser. Journal of Laser Applications, 35(4).

[9] Gong, J., Peng, G., et al., 2021. "Effect of plasma plume produced by vacuum laser welding on energy transmission," Optics & Laser Technology, Vol. 136, pp. 106744, ISSN 0030-3992.

[10] Cai C, Peng G C, Li L Q, et al. 2014. Comparative study on laser welding characteristics of aluminium alloy under atmospheric and subatmospheric pressures [J]. Science and Technology of Welding and Joining, 19(7): 547-553.

[11] Jiang, Y., Jiang, M., Chen, X., Chen, A., Ma, S. ,& Jiang, N., et al. (2024). Vacuum laser beam welding of az31 magnesium alloy: weld formability, microstructure and mechanical properties. Optics and Laser Technology, 169.

[12] Ma, D., Jiang, P., Shu, L., Qiu, Y., Zhang, Y., & Geng, S.. (2023). Dbn-based online identification of porosity regions during laser welding of aluminum alloys using coherent optical diagnosis. Optics & Laser Technology.

[13] Li, L., Peng, G., Wang, J., Gong, J., & Meng, S.. (2019). Numerical and experimental study on keyhole and melt flow dynamics during laser welding of aluminium alloys under subatmospheric pressures. International Journal of Heat and Mass Transfer, 133, 812-826.

[14] Fabbro R, Hirano K, Pang Shengyong. 2016. Analysis of the physical processes occurring during deep penetration laser welding under reduced pressure[J]. Journal of Laser Applications, 28(2): 022427.

[15] Huang, YW., Gao, XD., Gao, P.P. et al. 2024. Laser welding monitoring techniques based on optical diagnosis and artificial intelligence: a review. Adv. Manuf. https://doi.org/10.1007/s40436-024-00493-1

[16] Cai W, Jiang P, Shu L et al. (2022) Real-time identification ofmolten pool and keyhole using a deep learning-based semantic segmentation approach in penetration status monitoring. J ManufProcess 76:695–707

[17] Sokolov M, Franciosa P, Sun T et al. (2021). Applying optical coherence tomography for weld depth monitoring in remote laser welding of automotive battery tab connectors. J Laser Appl 33:012028. https:// doi. org/ 10. 2351/7. 00003 36